A Simplified Evaluation Framework for Adaptation Measures to Urban Heat Islands

Takebayashi, Hideki

(Citation)
Buildings,14(8):2417

(Issue Date)
2024-08

(Resource Type)
journal article

(Version)
Version of Record

buildings

MDPI

Article

A Simplified Evaluation Framework for Adaptation Measures to Urban Heat Islands

Hideki Takebayashi

Department of Architecture, Graduate School of Engineering, Kobe University, Kobe 657-8501, Japan; thideki@kobe-u.ac.jp; Tel.: +81-78-803-6062

Abstract: Adaptation measures to urban heat islands are classified into the following three categories: measures to reduce solar radiation incident on the human body, measures to control and cool ground and wall surface temperature, and measures to control and cool the air and human body temperature. Case studies are conducted to evaluate the effects of the implementation of a cool water circulation sunshade and to examine the adverse effects of cool pavements on the human thermal environment, in addition to the effects of mist sprays on the human body. The effect of the sunshade, watering road, and mist spray, which are typical adaptation measures to urban heat islands, on the human thermal environment was estimated using Wet Bulb Globe Temperature (WBGT) as an indicator for heat stroke prevention and Standard New Effective Temperature (SET*) as an indicator for thermal comfort assessment. The effect of solar radiation shielding on improving the human thermal environment was the most significant, with a large decrease in the amount of solar radiation absorbed by the human body, resulting in a large decrease in SET* and WBGT of 2.7 °C and 1.0 °C, respectively, on fine summer days.

Keywords: adaptation measure; urban heat island; outdoor human thermal environment; mist spray; sunshade; watering road

Citation: Takebayashi, H. A Simplified Evaluation Framework for Adaptation Measures to Urban Heat Islands. *Buildings* **2024**, *14*, 2417. https://doi.org/10.3390/buildings14082417

Academic Editor: Yupeng Wang

Received: 10 June 2024
Revised: 2 August 2024
Accepted: 4 August 2024
Published: 5 August 2024

1. Introduction

In recent years, in order to serve as effective solutions to outdoor human thermal environments under the influence of urban heat islands, adaptation measures, such as awnings, louvers, directional reflective materials, mist sprays, and evaporative materials, have been developed. For example, Rossi et al. [1,2] proposed an optimized awning with aluminized polyester film and evaluated it using the modified Physiological Equivalent Temperature. They considered the Effective Temperature (ET), the Corrected Effective Temperature (CET), the Wet Bulb Globe Temperature (WBGT), the Predicted Mean Vote (PMV), the Universal Thermal Climate Index (UTCI), the Physiologically Equivalent Temperature (PET), and other thermal environment indices, and determined that the PET was appropriate for their evaluation.

Sakai et al. [3] proposed a fractal-shaped sunshade consisting of many Sierpinski tetrahedron units and tested it in some full-scale experiments; then, they showed that fractal-shaped sunshades provide a comfortable environment and significantly reduce heat stress in urban areas. They discussed the effectiveness of those sunshades by decreasing the ground surface temperature under the sunshades.

Coutts et al. [4] evaluated the effects of street trees on human thermal comfort in the street canyon. Takebayashi et al. [5] evaluated the effects of solar radiation shading by trees in the open space around buildings. Zhao et al. [6] presented the tree shade benefits for residential outdoor thermal environments. Lee et al. [7] studied the effects of solar shading in walking spaces, focusing on sunny and shade conditions. Morakinyo et al. [8] compared the cooling efficacy of natural and artificial shading devices on very hot days. Elgheznawy and Eltarabily [9] investigated the impact of sun-sail shading on thermal comfort in school

courtyards. Middle et al. [10] conducted field measurements to quantify the efficacy of various shade types. Ou and Lin [11] examined the effects of orientation and dimensions of shading structures on thermal comfort in subtropical Taiwan. The effective aspect ratio was developed for shading evaluation. Lam et al. [12] evaluated the effects of shading devices on outdoor thermal and visual comfort. Heidari et al. [13] reported that awnings could reduce PET and UTCI by 3.34 °C and 2.14 °C, respectively.

Highly reflective pavements and water-retentive pavements have been considered as road measures [14,15]. A continuous water supply is required to ensure a stable evaporative cooling effect on water-retentive pavements. Continuous water supply systems are commercially available [16], but they are very expensive and time-consuming to manage. The effect of cool pavements is mainly related to reflection and evaporation, with smaller effects from heat storage [17]. Anand et al. [18] point out that heat storage is effective when thermal comfort during the day is a priority, but it can also cause heat islands at night. Hendel et al. found that watering reduced the surface temperature by 4 °C in the shade and 13 °C in the sun, as measured by an infrared camera [19]. Asaeda et al. focused on heat storage and investigated the heat balance in several pavement types [20]. Qin and Hiller focused on thermal inertia and investigated the heat balance of pavement surfaces [21]. Broadbent et al. evaluated the potential cooling effects of irrigation [22]. Gao and Santamouris investigated the temperature reduction due to irrigation and noted the need to optimize irrigation [23]. Daniel et al. analyzed the cooling effects of watering vegetation and irrigating pavement [24]. Hendel et al. studied the optimization of watering methods for pavements [25]. Wei and He studied numerical simulations to analyze the thermal improvement effects of evaporative cooling on urban surfaces [26]. Djekic et al. discussed the relationship between color, roughness, and shading of several materials and surface temperature and found that human thermal comfort is dominated by the effect of shading [27]. Wang et al. reported that watering can reduce surface temperature and wet bulb globe temperature (WBGT) at a height of 0.5 m from cold pavement by up to 10 °C and 2 °C, respectively [28]. The heat balance of the pavement surface has also been analyzed [29,30]. In addition, the surface temperature reduction effects of various types of water-retentive pavements have been investigated using field observations [16,31–36]. Recently, a field study on the thermal environmental mitigation effects of road sprinkling was conducted in Paris, France [37].

Nouri et al. [38] reviewed overall existing approaches to pedestrian thermal comfort thresholds and the different techniques and measures. Shooshtarian et al. [39] reviewed the critical analysis of the literature on thermal adaptive strategies in outdoor spaces. Lai et al. [40] reviewed the effects of using geometry, vegetation, cool surfaces, and water bodies for the thermal environment and thermal comfort in urban outdoor spaces. They stated that the effects of the strategies are better in hotter and drier climates, and also reported that reflective surfaces increased PET. Takebayashi and Kyogoku [41] evaluated the radiation environment focusing on ground cover materials and solar radiation shading. Karimi et al. [42] analyzed the effects of albedo and vegetation coverage on thermal comfort in a medium-sized urban park using ENVI-met software (version 4.3.2). They pointed out that the effect of albedo on thermal comfort was lower than that of vegetation coverage.

Ulpiani [43] reviewed studies on the effects of mist spraying and organized the cooling effect of air temperature by mist spraying. In her review, mainly air temperature decrease and humidity increase were organized, but evaluations by WBGT, ET*, SET*, UTCI, and PMV were also presented. The Japanese Ministry of the Environment [44] developed the 'Heat countermeasure guideline in the city'. In the guideline, adaptation measures are classified into the following categories: solar radiation shielding (top), ground surface heat control/cooling (bottom), wall surface heat control/cooling (side), and air/body cooling (middle). The effects of each measure on the reduction of heat index (WBGT, Wet Bulb Globe Temperature) and sensible temperature (SET*, Standard New Effective Temperature) are summarized.

As mentioned above, various thermal environment indices are used to evaluate the thermal environment of outdoor spaces. In this study, the WBGT and SET* adopted in the Japanese guideline were used for evaluation. Takebayashi et al. [45,46] have conducted measurement and simulation studies of the effects of sunshades, mist spraying, water sprinkling, water surfaces, etc., in cooperation with Kobe City, one Japanese local government. It was pointed out that it is necessary to appropriately select each technology based on the characteristics of the target space because the effect of improving the human thermal sensation varies depending on the distance from the countermeasure technology to the human body. Then, Kobe City [47–50] began to actively adopt them in redevelopment projects in front of its main station. Sunshades, mist sprays, water surfaces, water sprinkling, greening, tree planting, ground surface cover improvement, and retroreflective technologies have already been practically introduced in Kobe City as countermeasures against the heat. Since the advanced efforts by Kobe City are of interest, at least domestically, it is necessary to develop a simple evaluation method for the effects of the implementation of these measures in order to expand their use to other regions.

Although a wide variety of technologies to improve the thermal environment of outdoor spaces and individual evaluation cases have been reported, it is necessary to organize a framework that enables mutual comparison of the effects of these technologies in order to apply them to actual society. Takebayashi [51] studied a simple evaluation method for solar radiation shielding and ground and wall surface cover improvement measures that are expected to be effective against heat. These measures correspond to the "top", "bottom", and "side" in the above-mentioned guideline classification. In this study, it was extended to "middle" and a simple method to evaluate the effect of mist spraying was examined. In particular, an evaluation framework for mist spraying and outdoor space cooling, which directly cools the air, needs to be considered for extension to "middle" evaluations. Oh et al. [52] evaluated an outdoor mist-spraying environment and its effect on thermal sensations, thermal environment, and skin temperature. Desert et al. [53] measured the spatial distribution of temperature and humidity around the mist spray and analyzed the relationship between human sensation and skin temperature. These studies suggest that the effectiveness of thermal environment improvement depends not only on the characteristics of the mist sprayer but also on its relationship with humans. Previous studies have not sufficiently investigated the evaluation based on the relationship between the countermeasure technology and the distance to the human body. In this study, I examined an evaluation framework that takes these factors into account.

Shimazaki et al. [54] evaluated human-thermal environments on water-retaining pavements with different reflectance by field measurements. They pointed out that an optimum value of solar reflectance existed for human thermal comfort. Therefore, it is required to quantitatively evaluate the negative effects of cool pavement with high reflectance. Takebayashi [51] pointed out that lowering the surface temperature of solar shields is effective in improving the human thermal environment. Therefore, a potential for development exists for solar radiation shields with lower surface temperatures. So, case studies were conducted to examine the adverse effects of cool pavements on the human thermal environment and to evaluate the effects of the implementation of a cool water circulation sunshade.

In this study, I examined measures to circulate water through the solar radiation shield, because previous studies have shown the importance of solar radiation shielding and the importance of not increasing the temperature of the shielded object. Since previous studies have pointed out the possibility that cool pavement may deteriorate the thermal environment of the human body, I analyzed the relationship between solar reflectance and thermal environment indices. Similarly, it has been pointed out that the effect of mist-spraying varies depending on the positional relationship between the mist-spraying device and the human body; so, I analyzed the relationship between the ventilation environment around the mist-spraying device and the effect of improving the thermal environment.

2. Evaluation Framework of Adaptation Measures for Urban Heat Island

In this study, a framework was organized to mutually evaluate their effectiveness in improving the thermal environment, using *SET** and *WBGT* as common thermal environment indices. In the 'Heat countermeasure guideline in the city' by the Japanese Ministry of the Environment [44], it was stated that the heat index (*WBGT*, Wet Bulb Globe Temperature [°C]) is a suitable indicator for heat stroke prevention and the sensitive temperature (*SET**, Standard New Effective Temperature [°C]) is a suitable indicator for thermal comfort assessment. Takebayashi [51] performed a sensitivity analysis of *SET** and reported the relationships between air temperature T_a [°C], humidity *RH* [%], X_a [g/kg'], wind speed v [m/s], mean radiant temperature *MRT* [°C] and *SET** as the following equations.

$$\Delta SET^*/\Delta T_a = 0.63, \tag{1}$$

$$\Delta SET^*/\Delta RH = 0.13, \quad \Delta SET^*/\Delta X_a = 0.43, \tag{2}$$

$$\Delta SET^*/\Delta v = 1.4, \tag{3}$$

$$\Delta SET^*/\Delta MRT = 0.21, \tag{4}$$

WBGT [°C] is calculated by Equation (5), where T_w is wet bulb temperature [°C] and T_g is black bulb temperature [°C]. The relationship between *MRT* and T_g is expressed in Equation (6) using wind speed v and air temperature T_a. Therefore, the change in black bulb temperature ΔT_g with changes in mean radiant temperature ΔMRT and air temperature ΔT_a is expressed by Equations (7) and (8).

$$WBGT = 0.7T_w + 0.2T_g + 0.1T_a, \tag{5}$$

$$MRT = T_g + 2.37v^{0.5}(T_g - T_a), \tag{6}$$

$$\Delta T_g = 1/(1 + 2.37v^{0.5})\Delta MRT = (0.3\sim0.5)\Delta MRT, \tag{7}$$

$$\Delta T_g = 2.37v^{0.5}/(1 + 2.37v^{0.5})\Delta T_a = (0.5\sim0.7)\Delta T_a, \tag{8}$$

The measures listed in the Japanese Ministry of the Environment's "Heat countermeasure guideline in the city" [44] are trees, pergolas, awnings, and retroreflective materials as "top"; evaporative pavement, reflective pavement, and green cover surfaces as "bottom"; green facades and louvers as "side"; and mist spray, fans, and cooling benches as "middle". As mentioned above, various adaptation measures are effective by improving different factors, such as solar radiation shielding to the human body, surface temperature reduction of ground and wall surfaces, and reduction of air and body surface temperatures.

The evaluation method for the "top" measures, i.e., measures to reduce solar radiation incidence, was explained in Section 2.1. It leads to the evaluation of *SET** and *WBGT* via ΔMRT, ΔT_g in Equations (4)–(7). The evaluation method for the "bottom" or "side" measures, i.e., measures to reduce infrared radiation incident on the human body from the ground or wall surfaces, was explained in Section 2.2. It leads to the evaluation of *SET** and *WBGT* via ΔMRT, ΔT_g in Equations (4)–(7). The evaluation method for the "middle" measures, i.e., measures to reduce the air temperature around the human body or the surface temperature of the human body, was explained in Section 2.3. It leads to the evaluation of *SET** and *WBGT* via ΔT_a, ΔX_a in Equations (1), (2), (5), (6) and (8). In the following Section 2.1 through Section 2.3, the evaluation methods for ΔT_a, ΔX_a, ΔMRT, and ΔT_g are explained for each technology group with different characteristics.

2.1. Measures to Reduce Solar Radiation

The Mean Radiation Temperature *MRT* [K] is calculated from Equation (9), considering solar radiation J [W/m^2] and infrared radiation $\varepsilon\sigma T_i^4$ [W/m^2] to the human body. The surface temperature T_s [°C] of the solar radiation shield is calculated by the heat budget equation in Equation (10) and is reflected in Equation (9). Direct, diffused, and reflected

solar radiation J_{dir}, J_{dif}, and J_{ref} [W/m^2] are included in the solar radiation incident on the human body J [W/m^2]. Transmittance τ [-] of the solar radiation shield is considered for direct solar radiation J_{dir} [W/m^2].

$$MRT = (a_h J/\varepsilon\sigma + \Sigma\Phi_i T_i^4)^{1/4}, \quad (9)$$

$$T_s = (aJ + \varepsilon q - lE)/\alpha + T_a, \quad (10)$$

$$J = J_{dir} + J_{dif} + J_{ref}, \quad (11)$$

where a_h is solar absorptance of the human body [-], ε is emissivity [-], σ is Stefan–Boltzmann constant 5.67 $\times$ 10^{-8} [W/(m^{2}K^4)], Φ_i is the view factor between the human body and objective surface [-], T_i is surface temperature [K], a is absorptance of solar radiation shield [-], q is atmospheric radiation [W/m^2], l is latent heat of water evaporation [J/g], E is evaporation flux [g/(m^{2}s)], α is convection heat transfer coefficient between solar radiation shield and air [W/(m^{2}K)], and T_a is air temperature [°C]. The main parameters are as follows (Figure 1):

- Absorptance and transmittance of the solar radiation shield a, τ [-];
- Evaporation flux E [g/(m^{2}s)] or evaporation efficiency β [-];
- Convection heat transfer coefficient α [W/(m^{2}K)];
- View factor between the human body and objective surface Φ [-].

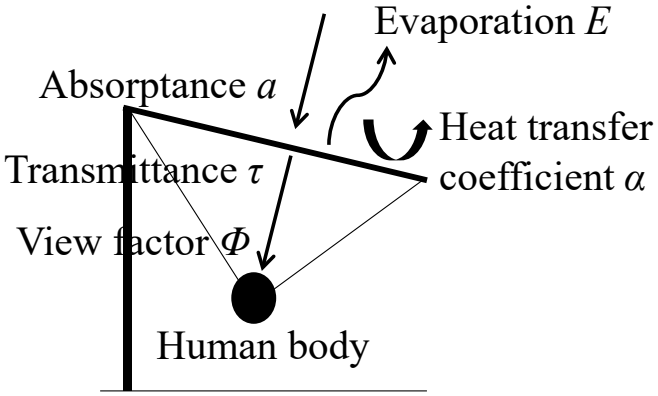

Figure 1. Main parameters of sunshade measure (a: solar radiation absorptance [-], τ: solar radiation transmittance [-], $\rho = 1 - a - \tau$: solar radiation reflectance [-], E: Evaporation flux [g/(m^{2}s)], α: convection heat transfer coefficient [W/(m^{2}K)], Φ: view factor between human body and objective surface [-]).

The implementation of these measures reduces the direct solar radiation J_{dir} [W/m^2] incident on the human body, thereby providing an effect of measures to prevent overheating. However, deterioration of the human thermal environment due to increased infrared radiation $\varepsilon\sigma T^4$ [W/m^2] from the solar radiation shield to the human body must be considered. The surface temperature T_s [°C] of the solar radiation shield does not increase when the solar radiation absorptance a [-] is small, i.e., when the solar radiation reflectance ρ [-] or transmittance τ [-] is large. In other cases, it is reduced by a large convective heat transfer coefficient α [W/(m^{2}K)], as in the case of a fractal-shaped sunshade [3], or by a large evaporative latent heat flux lE [W/m^2] by supplying water. The study results of changing these parameters (a, τ, E, α, Φ) were reported in a previous study by Takebayashi [51]. If the solar radiation shield covers the entire upper space of the human body, $\Phi = 0.5$. In an open space such as a plaza unaffected by surrounding buildings, if the definition of the sky view factor SVF is $SVF = 1$ if all the sky is visible, then $SVF = (0.5 - \Phi) \times 2$.

2.2. Measures to Cool Ground and Wall Surface Temperature

It is mainly evaluated based on the radiation and heat budget on the objective surface. The surface heat budget equation is as follows.

$$S + R = V + A + lE, \tag{12}$$

$$S = (1 - \rho)\, J, \tag{13}$$

$$R = R\downarrow - \varepsilon\delta {T_s}^4, \tag{14}$$

$$V = \alpha_c\, (T_s - T_a), \tag{15}$$

$$A = -\lambda \partial T / \partial z, \tag{16}$$

$$lE = l\beta\alpha_w\, (X_s - X_a), \tag{17}$$

$$R\downarrow = \sigma {T_a}^4\, (0.526 + 0.208\sqrt{P}), \tag{18}$$

$$\alpha_c = 5.3 + 3.6u\ (u \leq 5.0) \text{ or } 6.47u^{0.78}\ (u \geq 5.0), \tag{19}$$

where S is solar radiation [W/m^2], R is infrared radiation [W/m^2], V is sensible heat flux [W/m^2], A is conduction heat flux [W/m^2], and lE is latent heat flux [W/m^2]. ρ is solar reflectance [-]. J [W/m^2] is incident solar radiation. $R\downarrow$ [W/m^2] is calculated by Brunt's formula (Equation (18)) using air temperature and relative humidity. ε is emissivity [-]. σ is Stefan–Boltzmann constant (=5.67 $\times$ 10^{-8} [W/(m^{2}K^4)]). T_s and T_a are surface and air temperature [K]. P is the water vapor pressure of air [kPa]. α_c is the convection heat transfer coefficient [W/(m^{2}K)], which is calculated by Jürges formula (Equation (19)) using wind velocity u [m/s]. T_s and T_a are surface and air temperatures [°C]. λ is the heat conductivity of the surface material [W/(mK)]. T [°C] is the temperature of the surface material, which is calculated by solving an unsteady one-dimensional heat conduction equation, to take thermal mass into account. l is the latent heat of water (=2500 [kJ/kg]). β is evaporative efficiency [-]. α_w is the convection moisture transfer coefficient [kg/(m^{2}s(kg/kg'))], which is calculated by the Lewis relation formula using α_c and specific heat of air. X_s and X_a are air absolute humidity and surface absolute humidity [kg/kg']. The main parameters are as follows (Figure 2):

- Solar reflectance ρ [-];
- Evaporation flux E [g/(m^{2}s)] or Evaporation efficiency β [-];
- View factor between the human body and objective surface Φ [-].

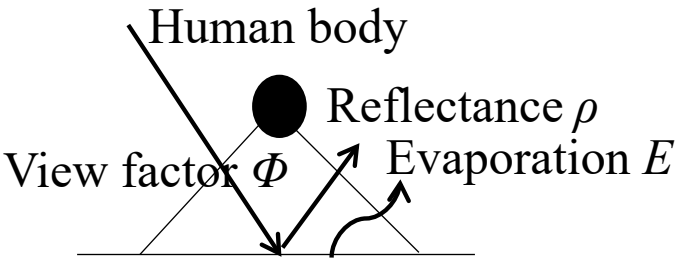

Figure 2. Main parameters of surface cooling measure (ρ: solar radiation reflectance [-], E: Evaporation flux [g/(m^{2}s)], Φ: view factor between human body and objective surface [-]).

The implementation of these measures reduces the infrared radiation $\varepsilon\sigma {T_s}^4$ [W/m^2] from the objective surface to the human body, thereby providing an effect of measures to prevent overheating. However, deterioration of the human thermal environment due to increased reflected solar radiation ρJ [W/m^2] must be considered. In the case of louvers placed next to the human body, a solar radiation shielding effect can be expected, but measures on the ground or wall surface do not reduce the amount of solar radiation incident on the human body, so the countermeasure effect against heat is not significant. In this examination, it is assumed that all of the sky is visible with a sky view factor of SVF = 1.

2.3. Measures to Cool Air Temperature and Human Body

Air temperature decrease ΔT_a [°C] and air humidity increase ΔX_a [g/kg′] due to mist spraying with spray rate Q [g/s] are calculated from Equations (20) and (21).

$$\Delta T_a = lQ/c_p \gamma n V, \quad (20)$$

$$\Delta X_a = c_p \Delta T_a / l, \quad (21)$$

where l is the latent heat of water evaporation [J/g], c_p is the specific heat of air [J/(gK)], γ is the density of air [g/m^3], n is air change rate [1/s], and V is the volume [m^3] of air in which mist evaporates. The main parameters are as follows (Figure 3):

- Spray rate Q [g/s];
- Air change rate n [1/s];
- Volume of air V [m^3].

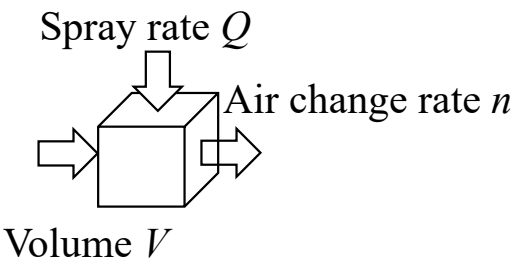

Figure 3. Main parameters of air-cooling measure (Q: spray rate [g/s], n: air change rate [1/s], V: volume of air [m^3]).

The implementation of mist spray decreases air temperature T_a [°C] and increases air humidity X_a [g/kg′] at constant enthalpy. The effect on the human thermal environment depends on the distance from the mist spray point to the human body and on the airflow conditions. In the case of airflow fans and outdoor cooling devices, the outlet temperature, humidity, and air speed from these devices are also defined, and their effects depend on the distance to the human body and the airflow conditions.

2.4. Evaluation Framework of Adaptation Measures

The evaluation methods in Section 2.1 to Section 2.3 are integrated into the evaluation framework of adaptation measures for urban heat islands shown in Figure 4. As a result, comparisons can be made under the same climatic conditions between countermeasure technologies with different characteristics, such as sunshade, greening, and misting.

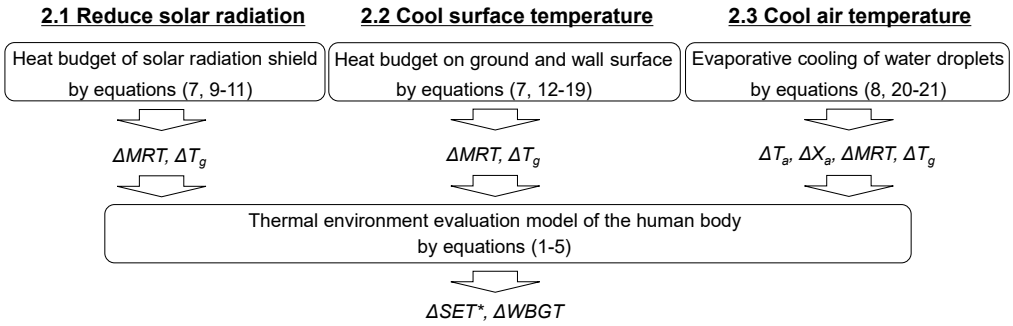

Figure 4. Evaluation framework of adaptation measures for urban heat island.

3. Case Studies

The evaluation framework was organized at the beginning of Chapter 2, followed by a description of the three groups of evaluation methods. In this chapter, specific examples are given and the main evaluation results are described. As described in the

introduction, three case studies were selected based on the issues from previous studies: solar shading with lowering surface temperatures, highly reflective pavement surfaces, and the distance between mist spray and the human body. Since the previous study by Takebayashi [51] has clarified the effects of changing the absorptance and transmittance, evaporation flux or evaporation efficiency, convective heat transfer coefficient, and view factor between the human body and the target surface of the solar radiation shield, which are the main parameters for evaluating the effectiveness of the countermeasure, Section 3.1 discusses the cool water circulation solar radiation shield as an advanced technology and explains the evaluation results. Previous studies have shown the effects of varying the reflectance, evaporative efficiency, thermal conductivity, and heat capacity of ground surfaces and walls, which are the main parameters for evaluating the effectiveness of countermeasures. However, it is necessary to evaluate the effects of increasing reflectance by integrating the decrease in infrared radiation and the increase in reflected solar radiation. Therefore, Section 3.2 discusses these relationships. Although the effects of mist spraying systems and outdoor air-cooling systems have already been clarified, the effects of thermal environment improvement vary depending on the positional relationship with the human body; therefore, Section 3.3 discusses evaluation cases focusing on these relationships. Through these verifications, it is believed that most of the major issues that need to be verified at this time have been covered.

3.1. Cool Water Circulation Sunshade

The effect of circulating water that is cooler than the air temperature in summer, such as in rivers and oceans, to reduce the temperature rise of solar radiation shields was studied. In particular, a cooler sunshade was proposed by circulating cold water on the sunshade panel surface before returning it to the aquifer of a cooling system that uses aquifer heat storage [55,56]. Figure 5 shows the hourly air and dew point temperatures observed at the Osaka meteorological observatory from April to October 2020. The black plots are measurements taken between 9:00 and 17:00. Since condensation occurs at temperatures below 25 °C during the summer daytime, the circulating water temperature for sunshade panels is assumed to be 25 °C in practical operation.

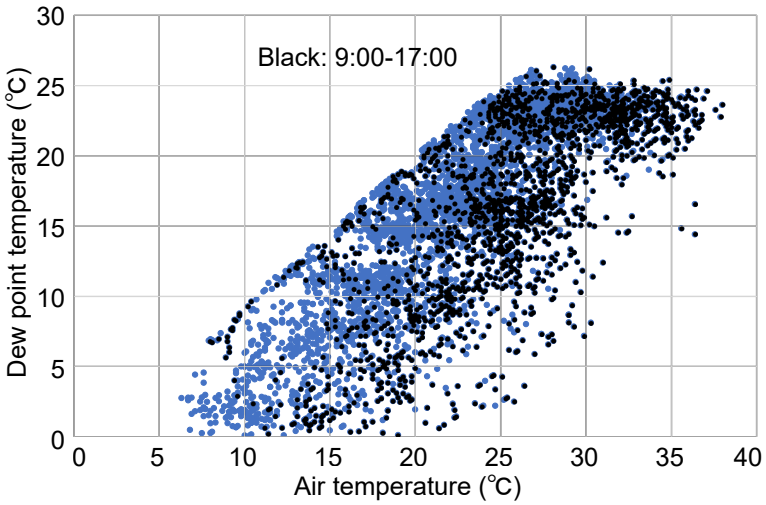

Figure 5. Hourly air and dew point temperatures observed at the Osaka meteorological observatory from April to October 2020. The black plots were measured during the day between 9:00 and 17:00. The blue plots were measured during the night.

Since the surface temperature of the sunshade without cold water circulation is calculated by Equation (2), the equivalent outside temperature T_e [°C] of the sunshade with cold water circulation is expressed by Equation (22), and the cold-water outlet temperature

T_{out} [°C] relative to the cold-water inlet temperature Tin [°C] and the heat loss from the sunshade panels Q [W/m^2] are calculated by Equations (23) and (24).

$$T_e = (aJ + \varepsilon q - lE)/\alpha + T_a, \quad (22)$$

$$T_{out} = T_e - (T_e - T_{in})e^{(-KAs/CG)}, \quad (23)$$

$$Q = CG(T_{out} - T_{in})/A_s, \quad (24)$$

where K is the heat loss coefficient of the sunshade [W/(m^{2}K)], A_s is the area of the sunshade [m^2], C is the specific heat of water [J/(kgK)], and G is the circulating water flow rate [kg/s]. The meteorological data were obtained from the Osaka meteorological observatory from April to October 2020.

Figure 6 shows the calculation result of outlet temperature, Tout, when the cold-water inlet temperature T_{in} = 25 °C, the area of the sunshade A_s = 100 m^2, the circulating water flow rate G = 1 kg/s (=60 L/min), the solar radiation absorptance of the sunshade a = 0.3, emissivity of the sunshade ε = 0.9, and the heat loss coefficient of the sunshade K = 3 W/(m^{2}K). The outlet temperature T_{out} increased to 26.5 °C, +1.5 °C compared to the inlet temperature T_{in} = 25 °C during the daytime (red plots), due to the absorption of solar radiation and dissipation of heat to the surrounding air (the heat loss from the sunshade panels Q = 60 W/m^2 at maximum), while it decreased to 23.5 °C (T_{in} − 1.5 °C) during the nighttime (blue plots) due to radiative cooling and dissipation of heat to the surrounding air. If a sufficient amount of water is supplied, the sunshade surface temperature is almost the same as the water supply temperature.

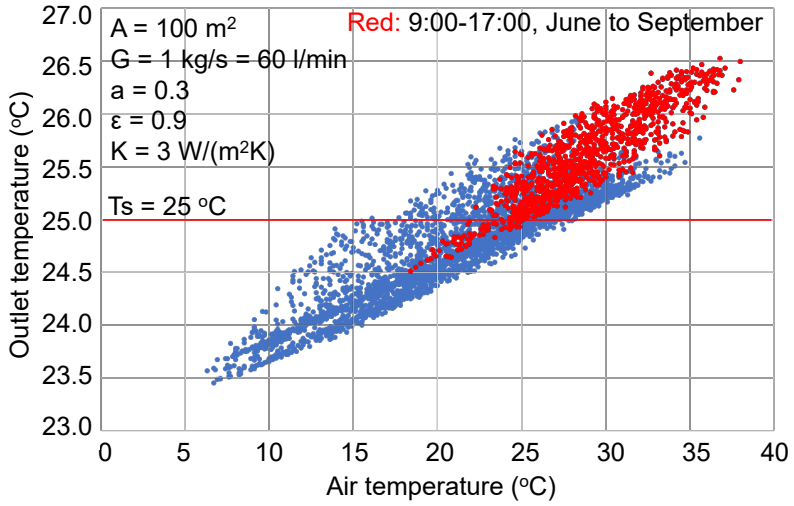

Figure 6. Calculation result of outlet temperature T_{out} when T_{in} = 25 °C, A_s = 100 m^2, G = 1 kg/s (=60 L/min), and a = 0.3, ε = 0.9, K = 3 W/(m^{2}K). Red plots are for daytime and blue plots are for nighttime.

Figure 7 shows the calculation results of outlet temperature T_{out} when the sunshade area A_s, the circulating water flow rate G, the solar radiation absorptance of the sunshade a, and the heat loss coefficient of the sunshade K are changed, in this case, the air temperatures are 15, 20, 25, 30, and 35 °C. The heat dissipation per unit area did not change when the sunshade area A_s was varied in the range shown in the horizontal axis of Figure 7, and was about −32.2, 3.7, and 39.7 W/m^2 at 15, 25, and 35 °C of outdoor air temperatures, respectively. The sunshade area A_s has a linear effect on the increase in outlet temperature T_{out}. The change in outlet temperature T_{out} is smaller as the circulating water flow rate G increases in the range shown in the horizontal axis of Figure 7. A stable cooling effect can be obtained if the circulating water flow rate G is kept above 1.0 kg/s, which is the reference value. The outlet temperature T_{out} increases as the solar radiation absorptance a increases in the range shown in the horizontal axis of Figure 7. At an outside air temperature of

35 °C, T_{out} = 26.0 °C for the reference condition a = 0.3, while T_{out} = 25.7 °C for white a = 0.1 and T_{out} = 26.6 °C for black a = 0.9. The outlet temperature T_{out} increases as the heat loss coefficient of the sunshade K increases in the range shown in the horizontal axis of Figure 7. At an outside air temperature of 35 °C, T_{out} = 26.0 °C for the reference condition K = 3 W/(m^{2}K), while T_{out} = 25.3 °C for K = 1 W/(m^{2}K) and T_{out} = 26.6 °C for K = 5 W/(m^{2}K). In conclusion, it can be considered that, if adequate circulating water flow rate G is provided within the expected sunshade area A_s, the effect of the cool water circulation sunshade can be achieved, although it is slightly affected by solar radiation absorptance a, emissivity ε, and heat loss coefficient K.

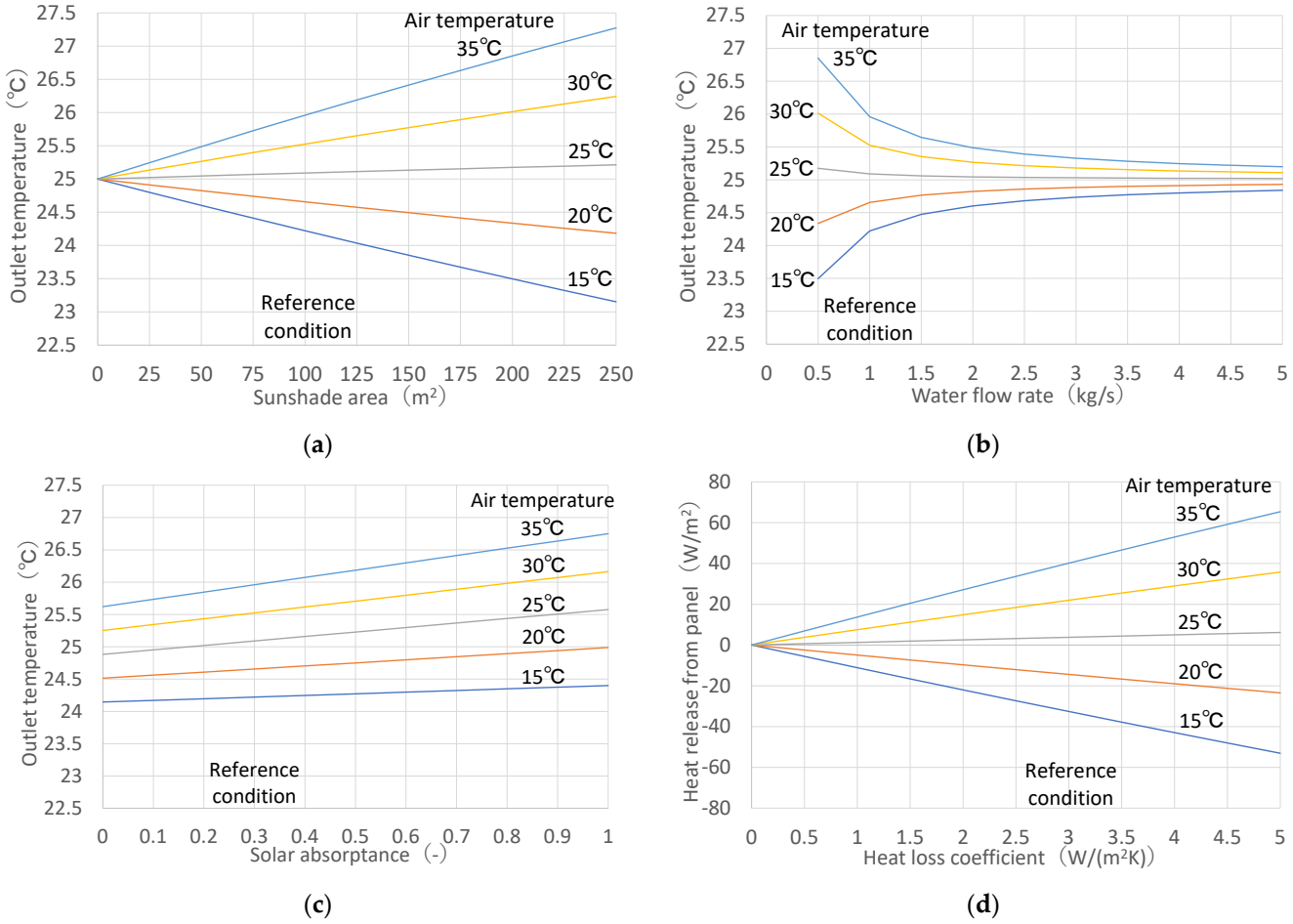

Figure 7. Calculation result of outlet temperature T_{out} when the sunshade area A_s [m^2], the circulating water flow rate G [kg/s], the solar radiation absorptance of the sunshade a [-], and the heat loss coefficient of the sunshade K [W/(m^{2}K)] are changed, in the case air temperature is 15, 20, 25, 30, and 35 °C. The reference conditions are A_s = 100 m^2, G = 1.0 kg/s, a = 0.3 and K = 3.0 W/(m^{2}K), respectively. (**a**) the sunshade area A_s [m^2] is changed; (**b**) the circulating water flow rate G [kg/s] is changed; (**c**) the solar absorptance a [-] is changed; (**d**) the heat loss coefficient K [W/(m^{2}K)] is changed.

Based on the above conditions, the *MRT* is calculated using Equation (9) and is shown in Figure 8. The *MRTs* in the case of no cool water circulation are organized in relation to the solar transmittance τ and absorptance a of the sunshade, in the case that evaporation on sunshade E = 0, view factor between sunshade and human body Φ = 0.3. Plots are shown for sunshades with from 18 °C to 38 °C cool water circulating over them. A sunshade with cool water circulating at 25 °C is slightly more effective than a white sunshade. Cool water circulation sunshades may have the potential to adapt to the heat if the supply of cool water as a renewable energy source is readily available [57].

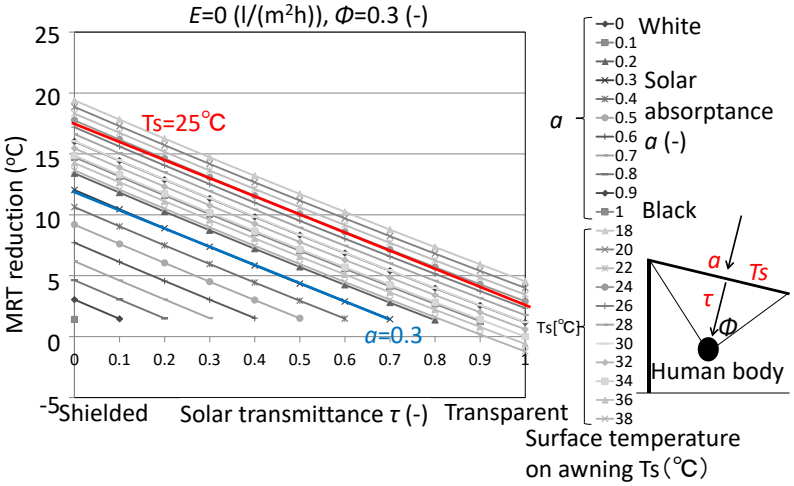

Figure 8. Solar transmittance τ [-], absorptance a [-], surface temperature Ts [°C] of the sunshade and MRT reduction [°C], when evaporation on sunshade E = 0, view factor between sunshade and human body Φ = 0.3. Surface temperature Ts of the sunshade is controlled by water circulation, while transmittance and absorptance of the sunshade are controlled by sunshade material.

3.2. Adverse Effects of Reflective Pavements on the Human Thermal Environment

Figure 9 shows the infrared radiation $\varepsilon\sigma T_s^4$ [W/m^2] from the ground surface calculated by the ground surface heat budget equation (Equation (12)) by changing the solar reflectance ρ on the ground surface. Emissivity ε, thermal conductivity λ, and heat capacity $c_{pg}\gamma_g$ were assumed to be 0.95, 0.74 W/(mK), and 2056 kJ/(m^{3}K), respectively, assuming asphalt. Observed data at the Osaka meteorological observatory, from 1 July to 30 September 2020, were given for the meteorological conditions. During the summer daytime, the ground surface temperature on the black surface exceeds 60 °C, so the infrared radiation may exceed 700 W/m^2. Calculations were conducted for evaporative efficiency β = 0.15 and solar reflectance ρ = 0.2, assuming a watering on the road. In this case, infrared radiation from the ground surface is comparable to that from the light-colored surface.

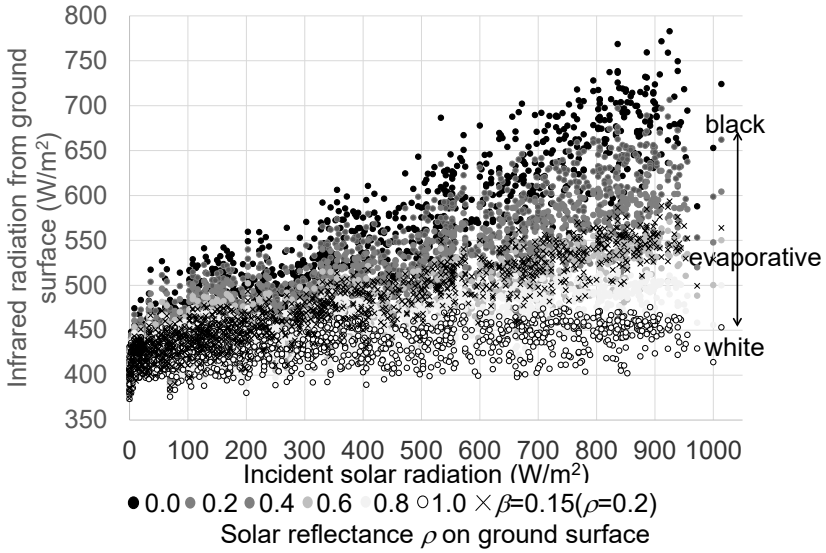

Figure 9. Infrared radiation $\varepsilon\sigma T_s^4$ [W/m^2] from ground surface by changing solar reflectance ρ [-] on ground surface, from July to September 2020 at Osaka meteorological observatory. Emissivity ε = 0.95, thermal conductivity λ = 0.74 W/(mK), and heat capacity $c_{pg}\gamma_g$ = 2056 kJ/(m^{3}K) were assumed for asphalt. Evaporative efficiency β = 0.15 and solar reflectance ρ = 0.2 were assumed for watering of the road.

Figure 10 shows *MRTs* for various human body's solar absorptance a_h by changing solar reflectance ρ on the ground surface, from 1 July to 30 September 2020 at Osaka meteorological observatory. Since the human body is strongly affected by reflected solar radiation from the ground surface when the human body's solar absorptance a_h is large, *MRT* is high on the ground surface where solar reflectance ρ is high. In other words, highly reflective cool pavement is not recommended when people are not wearing bright clothing. When the human body's solar absorptance a_h is below 0.25, this means that the adverse effects of reflected solar radiation from the ground surface are not confirmed when people wear white clothing. However, in this case, the increase in reflected solar radiation associated with the increase in ground surface solar reflectance and the decrease in infrared radiation associated with the decrease in surface temperature is almost offset. Therefore, although the adverse effects of reflected solar radiation can be avoided if people wear white clothing, changing to a highly reflective cool pavement cannot improve the thermal environment of the human body. However, as shown in Figure 10d, when the reflected solar radiation from the ground surface is zero, the highly reflective cool pavement is effective even if people wear dark-colored clothing. If highly reflective pavement surfaces that reflect only in specific directions, even when subject to abrasion by vehicles and people, can be easily introduced, there is potential for highly reflective cool pavement not only as a heat island mitigation measure but also as an adaptation measure. However, in the present conditions, when high reflectance paint is applied to asphalt pavement surfaces, which are composed of aggregates with various shapes, the reflected solar radiation is reflected in various directions. Compared to the directional reflection ground surface case, the *MRT* reduction effect is greater when the person is under a sunshade such as a parasol, as shown in Figure 10e. It is essential to promote public knowledge of the importance of more personal clothing and sun-shading umbrellas. Note that the view factors are 0.5 for the upper sky and the ground surface, and change to 0.3 for the sunshade (0.2 for the upper sky).

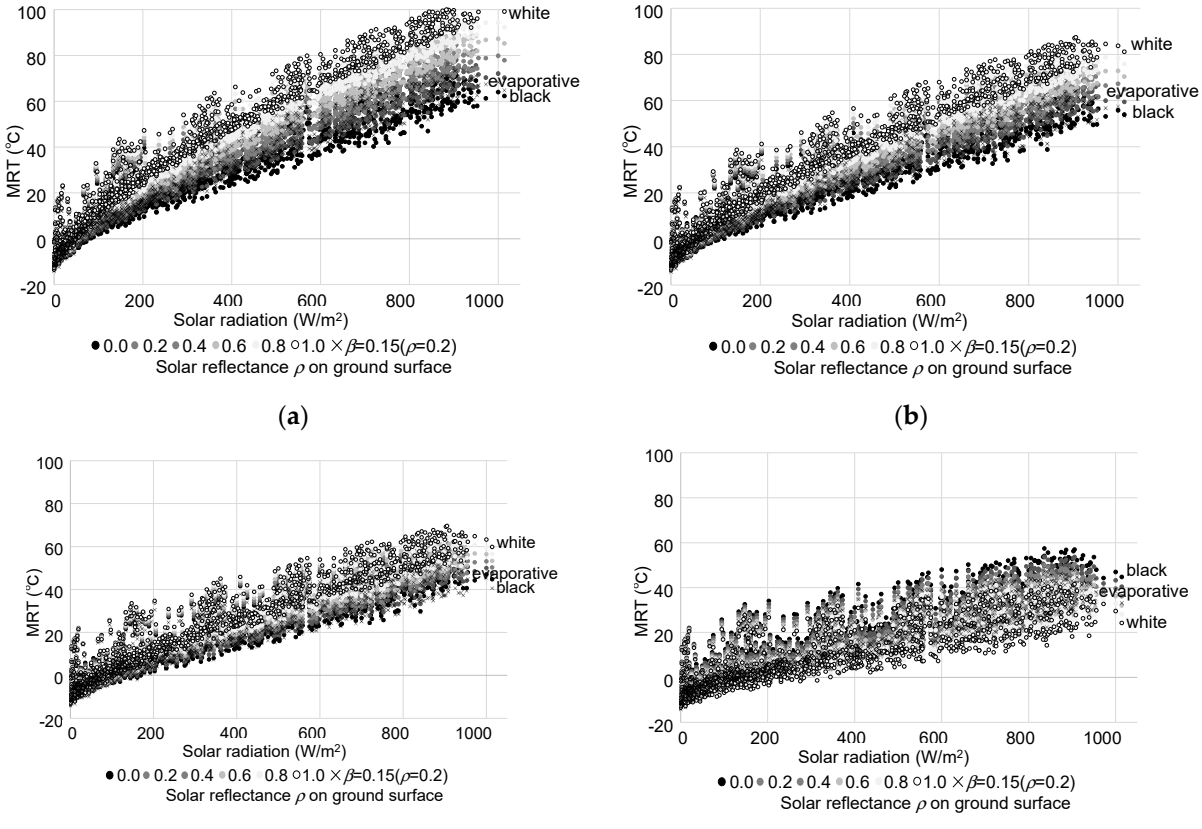

Figure 10. *Cont.*

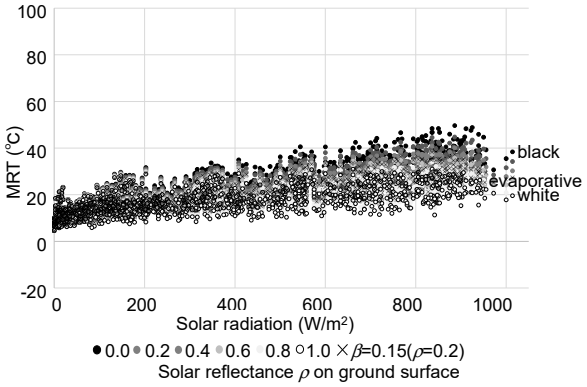

(**e**)

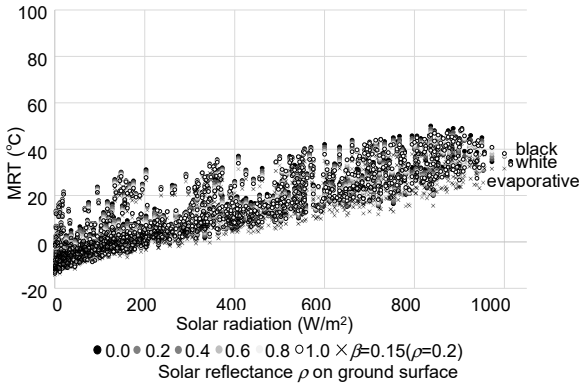

(**f**)

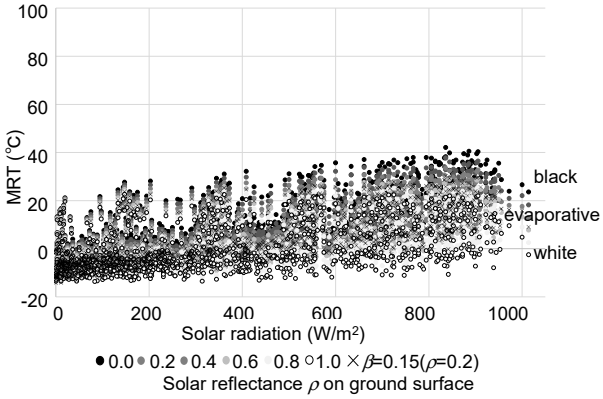

(**g**)

Figure 10. *MRTs* for various human body's solar absorptance a_h [-] by changing solar reflectance ρ [-] on ground surface, from July to September 2020 at Osaka meteorological observatory. Emissivity ε = 0.95, thermal conductivity λ = 0.74 W/(mK), and heat capacity $c_{pg}\gamma_g$ = 2056 kJ/(m^{3}K) were assumed for asphalt. Evaporative efficiency β = 0.15 and solar reflectance ρ = 0.2 were assumed for watering of the road. (**a**) Human body's solar absorptance a_h = 1.0 (black clothes); (**b**) a_h = 0.75 (dark gray clothes); (**c**) a_h = 0.5 (gray clothes); (**d**) a_h = 0.5 without reflective solar radiation from ground; (**e**) a_h = 0.5 with sunshade (incident solar radiation to the human body is 0); (**f**) a_h = 0.25 (light gray clothes); (**g**) a_h = 0.0 (white clothes).

3.3. Mist Splay Effects on the Human Body

Assuming that all the sprayed water evaporates in V = 0.5 × 0.5 × 0.5 [m^3] and the air is exchanged at a horizontal wind velocity of 1.0 [m/s], then ΔT_a = 2500 Q/(1.0 × 1200 × 1.0 × 0.5 × 0.5) = 8 Q [K] from Equation (20). If the spray rate Q = 1.0 [g/s] (=60 [mL/min]), ΔT_a = −8 [K], and ΔX_a = +3.2 [g/kg'] around the spray outlet. The air cooled and humidified by the mist spray is advected and diffused into the surrounding area. Those conditions are generally governed by the airflow field, except for the buoyancy effect due to temperature differences. Therefore, when the airflow field (u, v, w: wind velocity components [m/s], K: turbulent diffusion coefficient [m^2/s] in Equation (25)) obtained by CFD is given, the following advection–diffusion equation (Equation (25)) is used to calculate the air temperature and humidity distributions ($\phi = T_a, X_a$).

$$\partial\varnothing/\partial t + u\partial\varnothing/\partial x + v\partial\varnothing/\partial y + w\partial\varnothing/\partial z = K\partial^2\varnothing/\partial x^2 + K\partial^2\varnothing/\partial y^2 + K\partial^2\varnothing/\partial z^2 \quad (25)$$

The effect on the human thermal environment depends on the distance from the mist spray point to the human body and on the airflow conditions. Similar to mist spraying, in the case of airflow fans and outdoor cooling devices, the outlet temperature, humidity, and wind velocity from these devices are also defined, and their effects depend on the distance

to the human body and the airflow conditions. Figure 11 shows the calculation results of air temperature and humidity vertical cross-section distribution when the mist is sprayed under the above assumptions for three typical public spaces (station plaza, park, and bus stop) where people stay. It is calculated by the so-called box model with mesh sizes of 0.5 m, 0.5 m, and 0.5 m. The airflow distribution is provided by calculation results that consider the building geometry using CFD [45]. The mist spraying effect can be evaluated under various conditions by changing the positional relationship between the mist spraying point and the human body, as well as the mist spraying rate. At a station plaza and a bus stop where mist is sprayed from 3 and 4 m above the ground, the cooling effect does not reach the human body on the ground due to the advection of the incoming wind, whereas, at a park where mist is sprayed from 0.65 m above the ground, the cooling effect reaches the human body on the ground.

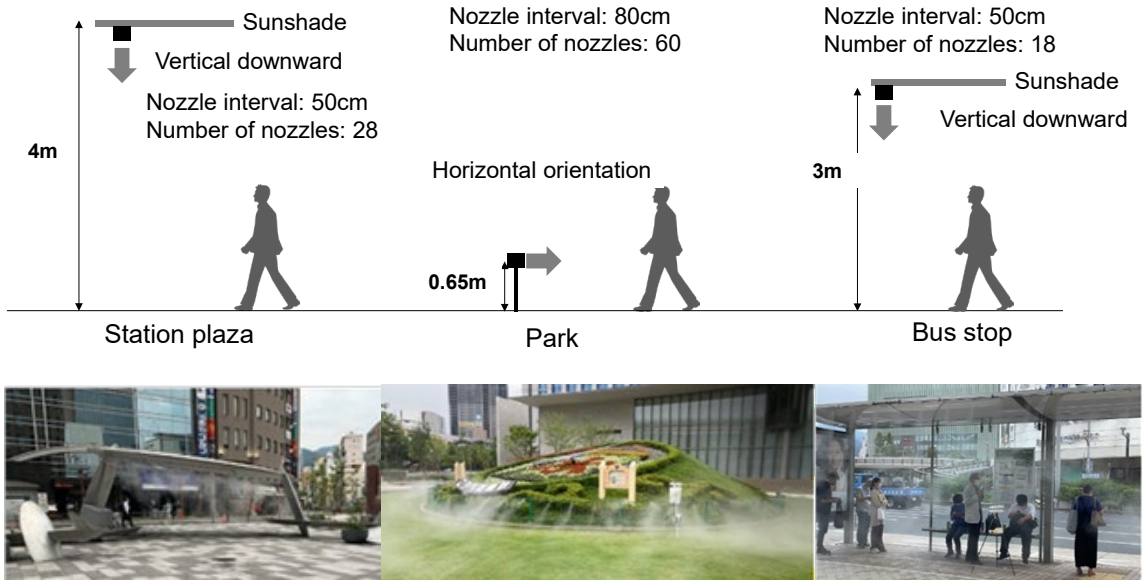

(**a**)

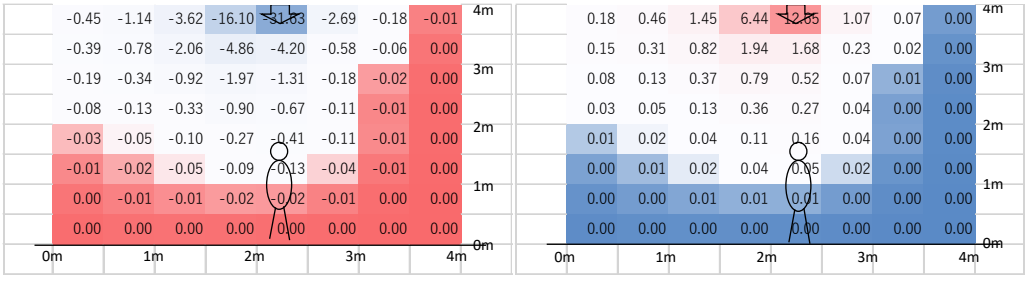

(**b**)

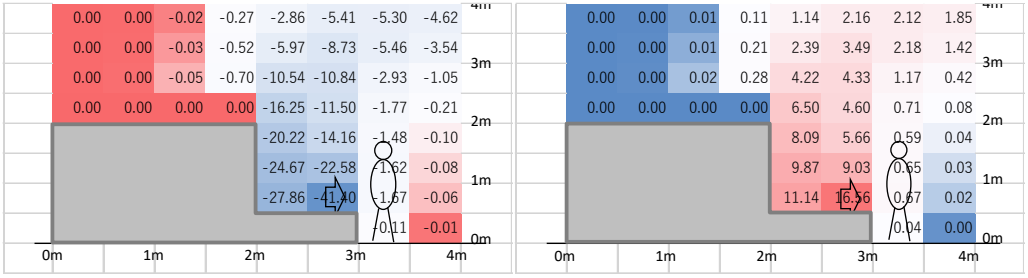

(**c**)

Figure 11. *Cont.*

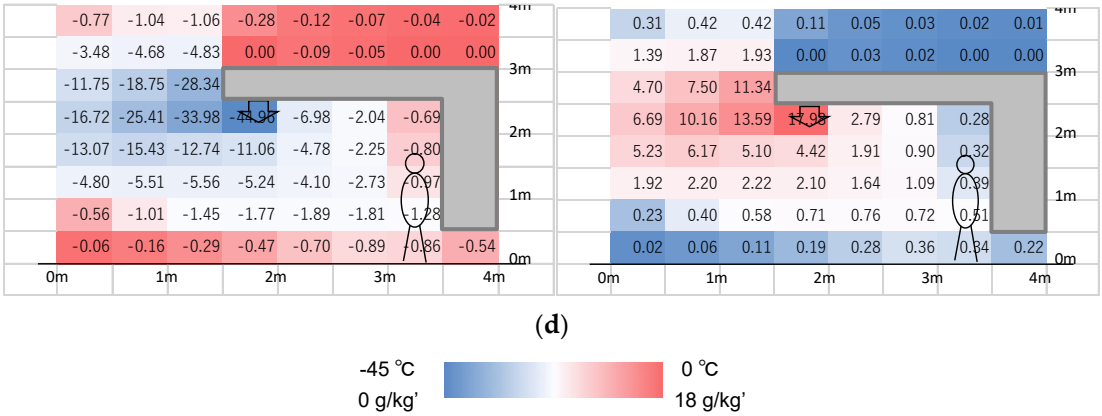

Figure 11. Calculation results of air temperature (left) and humidity (right) vertical cross-section distribution influenced by mist spraying (spray rate: Q = 1.0 g/s, wind velocity: v = 1.0 m/s, mesh size: 0.5 m, 0.5 m, 0.5 m). At the arrow point in each figure, $\Delta T_a = -8$ [K] and $\Delta X_a = +3.2$ [g/kg'] around the spray outlet are set for the airflow distribution calculation, assuming that all the sprayed water evaporates in V = 0.5 m × 0.5 m × 0.5 m. (**a**) Mist spraying at a station plaza, park, and bus stop (upper: photograph, lower: cross-section). At the station plaza and bus stop, people are assumed to be at the bottom of the mist, and, at the park, people are assumed to be close to the mist. (**b**) Mist spraying at a station plaza. Mist is sprayed and evaporated at the arrow point, and the human body is typically in the human body position. Wind velocity v = 1.0 m/s flows in from the right side of the figure. (**c**) Mist spraying at a park. Mist is sprayed and evaporated at the arrow point, and the human body is typically in the human body position. Wind velocity v = 1.0 m/s flows in from the right side of the figure. (**d**) Mist spraying at a bus stop. Mist is sprayed and evaporated at the arrow point, and the human body is typically in the human body position. Wind velocity v = 1.0 m/s flows in from the right side of the figure.

In this calculation method, the airflow field is determined by the influence of weather conditions and obstacles such as surrounding buildings, structures, and trees, but the influence of the blowing jet by the mist spraying device itself is not considered. Additionally, as a big problem, it is assumed that the water droplets blown out from the mist spraying equipment all evaporate in the calculation grid in the vicinity, and the air temperature drops and humidity rises. In practice, there is a possibility of evaporation in the grids other than the calculation grid in the vicinity, and it has been confirmed that the water droplet reaches the ground surface without evaporation when it is large. In this calculation, it was assumed that the mist particle shape was sufficiently small, that the mist evaporated near the mist device, and that the air temperature-lowering effect and the humidity-rising effect were passively transmitted by the wind flow. Since the CFD reproduced the unsteady field by the LES model, it became possible for engineers in Kobe City who are considering the introduction of mist spraying to design appropriate installation conditions of mist devices assuming various weather conditions.

4. Discussion

In the case of the sunshade, the amount of solar radiation absorbed by the human body is reduced by about 100 W/m^2, *MRT* is reduced by about 13 °C [51], *SET** by about 0.21 × 13 = 2.7 °C (Equation (4)), and *WBGT* by about 0.2 × 0.4 × 13 = 1.0 °C (Equations (5) and (7)). Meng et al. [58] reported that the *MRT* of the children on the school road was decreased by up to 21.25 °C by the shade of the building, and it also decreased by about 10 °C at other times. It is pointed out that the effect of street trees is less than 10 °C. A relatively large decrease in *SET** and *WBGT* can be expected when calculated in the same manner as above. In general, underground temperatures have smaller fluctuations than surface temperatures, so, in climatic zones with hot and cold seasons, there is a possibility of using cooler underground temperatures during the hot season. Water temperature

fluctuations are also smaller than surface temperature fluctuations, so there is a possibility of using cooler water temperatures during the hot season if the water is obtained from an appropriately deep location. Although this study presents the results of a case study under specific climatic conditions, it is possible to discuss the possibility of extending the study to other regions by conducting similar studies.

In the case of watering the road surface, the road surface temperature decreased by about 10 °C, *MRT* on the adjacent sidewalks decreased by about 2.4 °C [8,11], *SET** by about 0.21 × 2.4 = 0.5 °C (Equation (4)), and *WBGT* by about 0.2 × 0.4 × 2.4 = 0.2 °C (Equations (5) and (7)). In the review paper by Seifeddine et al. [59], the effect of water-retaining pavements which can hold water for relatively long evaporation was reported to decrease the surface temperature by up to 13 °C during the day, and the effect of about 20 °C was even larger depending on the water supply condition in other studies. Though the lowering effect of *SET** and *WBGT* can be predicted by the calculation in the same way as above, the integrated effect is not large only due to the lowering effect of the ground surface temperature at the foot. Incident solar radiation at different times of the day from summer to autumn in a particular city was used for the case studies. Thus, the incident solar radiation is widely varied from 0 to 1000 W/m^2. While the meteorological factors of air temperature, humidity, and wind velocity are meteorological conditions in a particular climate zone, the dominant factor in this study is the incident solar radiation, so the results can be shared over a wider area.

In the case of mist spray, air temperature T_a decreases by about 2.0 °C, air humidity X_a increases by about 0.8 g/kg', and the relative humidity *RH* increases by about 2.4% [23,24], *SET** by about 0.63 × 2.0 − 0.13 × 2.4 = 0.9 °C (Equations (1) and (2)), and *WBGT* by about 0.2 × 0.6 × 2.0 + 0.1 × 2.0 = 0.4 °C (Equations (5) and (8)). In this case, the wet bulb temperature T_w does not change because of the constant enthalpy change. According to the review of Ulpiani [43], there is a large variation in the air temperature lowering effect and humidity raising effect according to the previous research. Variations are also pointed out by measurement results and numerical calculations. Unfortunately, it is difficult to prepare a comparable situation by controlling weather conditions, etc., based on actual usage. Depending on the positional relationship between the mist spraying equipment and the measuring point, the effect of an air temperature drop of from several to 10 °C is often reported. It is difficult to specify the humidity rise because there are some cases that have not been measured. In view of this situation, since the spray rate Q can be confirmed by mist manufacturers, the method proposed in this study to predict air temperature and humidity distribution given the spray rate Q and weather conditions (u, v, w) is considered to be a realistic strategy. If the weather conditions are high *RH*, the volume of water available for evaporation is limited, so not all of the sprayed water droplets represented by the spray rate Q will evaporate, potentially wetting the ground, walls, and human bodies directly.

Examples of these typical adaptation effects are summarized in Table 1. Although the effectiveness of each technology varies depending on the local conditions and weather conditions of the installation site, it is recognized that the contents of the table reflect general trends based on the results of previous studies.

Table 1. Example of typical adaptation measures effects.

	Change of *MRT*, T_a, X_a	***SET** Reduction**	***WBGT* Reduction**
Sunshade	*MRT* − 13 °C	2.7 °C	1.0 °C
Watering road	*MRT* − 2.4 °C	0.5 °C	0.2 °C
Mist spray	T_a − 2 °C, X_a + 0.8 g/kg'	0.9 °C	0.4 °C

5. Conclusions

In this study, a simplified evaluation framework for adaptation measures to urban heat islands is examined. Case studies are conducted to evaluate the effects of the implementation of a cool water circulation sunshade and to examine the adverse effects of cool pavements on the human thermal environment, in addition to the effects of mist sprays

on the human body. The effect of the sunshade, watering road, and mist spray, which are typical adaptation measures to urban heat islands, on the human thermal environment was estimated using *WBGT* as an indicator for heat stroke prevention and *SET** as an indicator for thermal comfort assessment. The main parameters for each category of adaptation measures are organized as follows, and it is possible to check the impact of each on the thermal environment indicators.

- Measures to reduce solar radiation incident on the human body: absorptance and transmittance of the solar radiation shield a, τ [-], evaporation flux E [g/(m^{2}s)] or evaporation efficiency β [-], convection heat transfer coefficient α [W/(m^{2}K)], and view factor between the human body and objective surface Φ [-].
- Measures to control and cool ground and wall surface temperatures: solar reflectance ρ [-], evaporation flux E [g/(m^{2}s)] or evaporation efficiency β [-], view factor between the human body and objective surface Φ [-].
- Measures to control and cool air temperature and the human body: spray rate Q [g/s], air change rate n [1/s], and volume of air V [m^3].

The following is an overall comparative study of these effects during the summer daytime. In the case of solar radiation shielding, the amount of solar radiation absorbed by the human body is reduced by about 100 W/m^2, and *MRT* decreases by about 13 °C, resulting in a large *SET** decrease of 2.7 °C and *WBGT* decrease of 1.0 °C. However, in the case of improved ground surface coverage, even if the ground surface temperature decreases by about 10 °C, *MRT* above the ground surface decreases by about 2.4 °C, resulting in *SET** decrease of only 0.5 °C and *WBGT* decrease of 0.2 °C. In the case of mist spraying, if air temperature decreases by about 2.0 °C, humidity increases by 0.8 g/kg', but *SET** decreases by 0.9 °C and *WBGT* decreases by 0.4 °C.

Since the fluctuation in underground temperature is less than that of the ground surface temperature, cooler underground temperatures may be available during the hot season in climatic zones that have hot and cold seasons. The fluctuation in water temperature is also smaller than that of the ground surface temperature, so, if water is obtained from an appropriately deep location, it can be used to lower temperatures on the solar radiation shading. However, as shown in this study, it is necessary to evaluate the risk of surface condensation depending on the climatic zone. Since the influence of high reflectance on ground surface coverage depends mainly on the incident solar radiation, the results of this study can be applied to different climatic zones with different air temperatures, humidities, wind velocities, etc., and the incident solar radiation can be considered as the main parameter. The effect of mist spray depends on the amount of evaporating water droplets and the subsequent diffusion conditions, so the cooling potential is smaller in humid climatic zones. The effect of wind velocity is influenced by local shielding around the spray area as well as climatic zones, so consideration of local effects is prioritized over climatic zones.

The effects of sunshades and the watering of roads are limited to the relationship between each measure and the location of the human body, but mist spraying requires more consideration of the spatial distribution of air temperature and humidity, so a so-called box model was presented to simply evaluate advection–diffusion by giving the wind velocity distribution as a boundary condition. For a more practical and effective introduction of countermeasures, it is necessary to consider an implementation plan that focuses on the positional relationship between countermeasure technology and the human body.

Funding: This work was supported by JSPS KAKENHI Grant Number JP22H01651 and the Taisei Foundation.

Data Availability Statement: The original contributions presented in the study are included in the article, further inquiries can be directed to the corresponding author.

Acknowledgments: The author thanks Ushio Tozawa and Saeko Osaki of Kobe City, and Masaki Nakao of Osaka Metropolitan University for their cooperation.

Conflicts of Interest: The author declares no conflicts of interest.

References

1. Rossi, F.; Cardinali, M.; Gambelli, A.M.; Filipponi, M.; Castellani, B.; Nicolini, A. Outdoor thermal comfort improvements due to innovative solar awning solutions: An experimental campaign. *Energy Build.* **2020**, *225*, 110341. [CrossRef]
2. Rossi, F.; Cardinali, M.; Giuseppe, A.D.; Castellani, B.; Nicolini, A. Outdoor thermal comfort improvement with advanced solar awnings: Subjective and objective survey. *Build. Environ.* **2022**, *215*, 108967. [CrossRef]
3. Sakai, S.; Nakamura, M.; Furuya, K.; Amemura, N.; Onishi, M.; Iizawa, I.; Nakata, J.; Yamaji, K.; Asano, R.; Tamotsu, K. Sierpinski's forest: New technology of cool roof with fractal shapes. *Energy Build.* **2012**, *55*, 28–34. [CrossRef]
4. Coutts, A.M.; White, E.C.; Tapper, N.J.; Beringer, J.; Livesley, S.J. Temperature and human thermal comfort effects of street trees across three contrasting street canyon environments. *Theor. Appl. Climatol.* **2016**, *124*, 55–68. [CrossRef]
5. Takebayashi, H.; Kasahara, M.; Tanabe, S.; Kouyama, M. Analysis of Solar Radiation Shading Effects by Trees in the Open Space around Buildings. *Sustainability* **2017**, *9*, 1398. [CrossRef]
6. Zhao, Q.; Sailor, D.J.; Wentz, E.A. Impact of tree locations and arrangements on outdoor microclimates and human thermal comfort in an urban residential environment. *Urban For. Urban Green.* **2018**, *32*, 81–91. [CrossRef]
7. Lee, L.S.H.; Cheung, P.K.; Fung, C.K.W.; Jim, C.Y. Improving street walkability: Biometeorological assessment of artificial-partial shade structures in summer sunny conditions. *Int. J. Biometeorol.* **2020**, *64*, 547–560. [CrossRef] [PubMed]
8. Morakinyo, T.E.; Ouyang, W.; Lau, K.K.L.; Ren, C.; Ng, E. Right tree, right place (urban canyon): Tree species selection approach for optimum urban heat mitigation—Development and evaluation. *Sci. Total Environ.* **2020**, *719*, 137461. [CrossRef] [PubMed]
9. Elgheznawy, D.; Eltarabily, S. The impact of sun sail-shading strategy on the thermal comfort in school courtyards. *Build. Environ.* **2021**, *202*, 108046. [CrossRef]
10. Middle, A.; Alkhaled, S.; Schneider, F.A.; Hagen, B.; Coseo, P. 50 Grades of Shade. *Bull. Am. Meteorol. Soc.* **2021**, *102*, E1805–E1820. [CrossRef]
11. Ou, H.Y.; Lin, T. Effects of orientation and dimensions of shading structures on thermal comfort. *Build. Environ.* **2023**, *243*, 110715. [CrossRef]
12. Lam, C.K.C.; Weng, J.; Liu, K.; Hang, J. The effects of shading devices on outdoor thermal and visual comfort in Southern China during summer. *Build. Environ.* **2023**, *228*, 109743. [CrossRef]
13. Heidari, A.; Davtalab, J.; Sargazi, M. Effect of awning on thermal comfort adjustment in open urban space using PET and UTCI indexes: A case study of Sistan region in Iran. *Sustain. Cities Soc.* **2024**, *101*, 105175. [CrossRef]
14. Scholz, M.; Grabowiecki, P. Review of permeable pavement systems. *Build. Environ.* **2007**, *42*, 3830–3836. [CrossRef]
15. Santamouris, M. Using cool pavements as a mitigation strategy to fight urban heat island—A review of the actual developments. *Renew. Sustain. Energy Rev.* **2013**, *26*, 224–240. [CrossRef]
16. Akagawa, H.; Komiya, H. Experimental study on pavement system with continuous wet surface. *J. Archit. Plann. Environ. Eng. AIJ* **2000**, *530*, 79–85. [CrossRef] [PubMed]
17. Qin, Y. A review on the development of cool pavements to mitigate urban heat island effect. *Renew. Sustain. Energy Rev.* **2015**, *52*, 445–459. [CrossRef]
18. Anand, J.; Sailor, D.J. Role of pavement radiative and thermal properties in reducing excess heat in cities. *Sol. Energy* **2022**, *242*, 413–423. [CrossRef]
19. Hendel, M.; Colombert, M.; Diab, Y.; Royon, L. Improving a pavement-watering method on the basis of pavement surface temperature measurements. *Urban Clim.* **2014**, *10*, 189–200. [CrossRef]
20. Asaeda, T.; Ca, V.; Wake, A. Heat storage of pavement and its effect on the lower atmosphere. *Atmos. Environ.* **1996**, *30*, 413–427. [CrossRef]
21. Qin, Y.; Hiller, J. Understanding pavement-surface energy balance and its implications on cool pavement development. *Energy Build.* **2014**, *85*, 389–399. [CrossRef]
22. Broadbent, A.M.; Coutts, A.M.; Tapper, N.J.; Demuzere, M. The cooling effect of irrigation on urban microclimate during heatwave conditions. *Urban Clim.* **2018**, *23*, 309–329. [CrossRef]
23. Gao, K.; Santamouris, M. The use of water irrigation to mitigate ambient overheating in the built environment: Recent progress. *Build. Environ.* **2019**, *164*, 106346. [CrossRef]
24. Daniel, M.; Lemonsu, A.; Viguié, V. Role of watering practices in large-scale urban planning strategies to face the heat-wave risk in future climate. *Urban Clim.* **2018**, *23*, 287–308. [CrossRef]
25. Hendel, M.; Colombert, M.; Diab, Y.; Royon, L. An analysis of pavement heat flux to optimize the water efficiency of a pavement-watering method. *Appl. Therm. Eng.* **2015**, *78*, 658–669. [CrossRef]
26. Wei, J.; He, J. Numerical simulation for analyzing the thermal improving effect of evaporative cooling urban surfaces on the urban built environment. *Appl. Therm. Eng.* **2013**, *51*, 144–154. [CrossRef]
27. Djekic, J.; Djukic, A.; Vukmirovic, M.; Djekic, P.; Brankovic, M. Thermal comfort of pedestrian spaces and the influence of pavement materials on warming up during summer. *Energy Build.* **2018**, *159*, 474–485. [CrossRef]
28. Wang, J.; Meng, Q.; Tan, K.; Zhang, L.; Zhang, Y. Experimental investigation on the influence of evaporative cooling of permeable pavements on outdoor thermal environment. *Build. Environ.* **2018**, *140*, 184–193. [CrossRef]
29. Asaeda, T.; Fujino, T. Heat flux and Heat storage Properties of the Paved ground. *J. Jpn. Soc. Hydrol. Water Resour.* **1992**, *5*, 3–7. [CrossRef]

30. Kinouchi, T.; Kanda, M. An observation on the climatic effect of watering on paved roads. *J. Hydrosci. Hydraul. Eng.* **1997**, *15*, 55–64. [CrossRef]
31. Ozaki, T.; Suzuki, Y. Study on the contribution of water-retentive ceramic tile to the reduction of environment heat accumulation. *J. Hydraul. Eng.* **1998**, *42*, 61–66. [CrossRef]
32. Yamagata, H.; Nasu, M.; Yoshizawa, M.; Miyamoto, A.; Minamiyama, M. Heat island mitigation using water retentive pavement sprinkled with reclaimed wastewater. *Water Sci. Technol.* **2008**, *57*, 763–771. [CrossRef] [PubMed]
33. Herb, W.; Janke, B.; Mohseni, O.; Stefan, H. Ground surface temperature simulation for different land covers. *J. Hydrol.* **2008**, *356*, 327–343. [CrossRef]
34. Akagawa, H.; Takebayashi, H.; Moriyama, M. Experimental study on improvement on human thermal environment on a watered pavement and a highly reflective pavement. *J. Environ. Eng. AIJ* **2008**, *73*, 85–91. [CrossRef]
35. Nakayama, T.; Fujita, T. Cooling effect of water-holding pavements made of new materials on water and heat budgets in urban areas. *Landsc. Urban Plan.* **2010**, *96*, 57–67. [CrossRef]
36. Yokota, K.; Yamaji, T.; Hirano, S. Basic characteristics of water permeable/retainable porous paving bricks for controlling urban heat island phenomenon. *J. Heat Isl. Inst. Int.* **2010**, *5*, 40–46.
37. Hendel, M.; Gutierrez, P.; Colombert, M.; Diab, Y.; Royon, L. Measuring the effects of urban heat island mitigation techniques in the field: Application to the case of pavement-watering in Paris. *Urban Clim.* **2016**, *16*, 43–58. [CrossRef]
38. Nouri, A.S.; Costa, J.P.; Santamouris, M.; Matzarakis, A. Approaches to outdoor thermal comfort thresholds through public space design: A review. *Atmosphere* **2018**, *9*, 108. [CrossRef]
39. Shooshtarian, S.; Rajagopalan, P.; Sagoo, A. A comprehensive review of thermal adaptive strategies in outdoor spaces. *Sustain. Cities Soc.* **2018**, *41*, 647–665. [CrossRef]
40. Lai, D.; Liu, W.; Gan, T.; Liu, K.; Chen, Q. A review of mitigating strategies to improve the thermal environment and thermal comfort in urban outdoor spaces. *Sci. Total Environ.* **2019**, *661*, 337–353. [CrossRef]
41. Takebayashi, H.; Kyogoku, S. Thermal Environmental Design in Outdoor Space Focusing on Radiation Environment Influenced by Ground Cover Material and Solar Shading, through the Examination on the Redevelopment Buildings in Front of Central Osaka Station. *Sustainability* **2018**, *10*, 337. [CrossRef]
42. Karimi, A.; Sanaieian, H.; Farhadi, H.; Norouzian-Maleki, S. Evaluation of the thermal indices and thermal comfort improvement by different vegetation species and materials in a medium-sized urban park. *Energy Rep.* **2020**, *6*, 1670–1684. [CrossRef]
43. Ulpiani, G. Water mist spray for outdoor cooling: A systematic review of technologies, methods and impacts. *Appl. Energy* **2019**, *254*, 113647. [CrossRef]
44. Ministry of the Environment Government of Japan. Heat Countermeasure Guideline in the City. Available online: https://www.wbgt.env.go.jp/pdf/city_gline/city_guideline_full.pdf (accessed on 26 September 2023).
45. Takebayashi, H.; Okubo, M.; Danno, H. Thermal Environment Map in Street Canyon for Implementing Extreme High Temperature Measures. *Atmosphere* **2020**, *11*, 550–562. [CrossRef]
46. Takebayashi, H.; Danno, H.; Tozawa, U. Study on appropriate heat mitigation technologies for urban block redevelopment based on demonstration experiments in Kobe city. *Energy Build.* **2021**, *250*, 111299. [CrossRef]
47. Takebayashi, H.; Danno, H.; Tozawa, U. Study on Strategies to Implement Adaptation Measures for Extreme High Temperatures into the Street Canyon. *Atmosphere* **2022**, *13*, 946. [CrossRef]
48. Kyogoku, S.; Takebayashi, H. Experimental Verification of Mist Cooling Effect in Front of Air-Conditioning Condenser Unit, Open Space, and Bus Stop. *Atmosphere* **2023**, *14*, 177. [CrossRef]
49. Kyogoku, S.; Takebayashi, H. Effects of Upward Reflective Film Applied to Window Glass on Indoor and Outdoor Thermal Environments in a Mid-Latitude City. *Sustainability* **2023**, *15*, 3848. [CrossRef]
50. Takebayashi, H.; Mori, H.; Tozawa, U. Study on An Effective Roadway Watering Scheme for Mitigating Pedestrian Thermal Comfort According to the Street Configuration. *Atmosphere* **2023**, *14*, 1014. [CrossRef]
51. Takebayashi, H. A simple method to evaluate adaptation measures for urban heat island. *Environments* **2018**, *5*, 70. [CrossRef]
52. Oh, W.; Ooka, R.; Nakano, J.; Kikumoto, H.; Ogawa, O. Evaluation of mist-spraying environment on thermal sensations, thermal environment, and skin temperature under different operation modes. *Build. Environ.* **2020**, *168*, 106484. [CrossRef]
53. Desert, A.; Naboni, E.; Garcia, D. The spatial comfort and thermal delight of outdoor misting installations in hot and humid extreme environments. *Build. Environ.* **2020**, *224*, 110202. [CrossRef]
54. Shimazaki, Y.; Aoki, M.; Karaki, K.; Yoshida, A. Improving outdoor human-thermal environment by optimizing the reflectance of water-retaining pavement through subjective field-based measurements. *Build. Environ.* **2022**, *210*, 108695. [CrossRef]
55. Yamamoto, S.; Nishioka, M.; Nabeshima, M.; Nakao, M.; Nakaso, Y.; Sakai, M.; Nakamura, K. Thermal energy storage air conditioning system utilizing aquifer, Performance study on air conditioning system combining direct use and heat source use with seasonal thermal energy storage. *J. Soc. Heat. Air-Cond. Sanit. Eng. Jpn.* **2017**, *248*, 1–9.
56. Nakao, M. Trends and practical scale demonstrations of aquifer thermal storage technology. *Dist. Heat. Cool.* **2018**, *120*, 18–24.
57. Nakao, M.; Nakai, M.; Nishioka, M.; Nabeshima, M.; Mori, N.; Yamochi, S. Use of thermal energy of bottom layer water in harbor during summer, Characteristics of vertical ocean water temperature distribution (part 1). In Proceedings of the Annual Conference of the Society of Heating, Air-Conditioning and Sanitary Engineers of Japan, Sendai, Japan, 12–14 September 2007; pp. 1733–1736.

58. Meng, Y.; Wang, J.; Xi, C.; Han, L.; Feng, Z.; Cao, S. Investigation of heat stress on urban roadways for commuting children and mitigation strategies from the perspective of urban design. *Urban Clim.* **2023**, *49*, 101564. [CrossRef]
59. Seifeddine, K.; Amziane, S.; Toussaint, E.; Ouldboukhitine, S. Review on thermal behavior of cool pavements. *Urban Clim.* **2023**, *51*, 101667. [CrossRef]